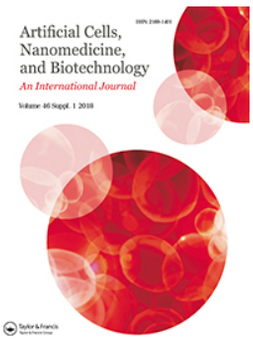

Taylor & Francis
Taylor & Francis Group

Artificial Cells, Nanomedicine, and Biotechnology

An International Journal

ISSN: 2169-1401 (Print) 2169-141X (Online) Journal homepage: http://www.tandfonline.com/loi/ianb20

Biodegradable composite porous poly(dl-lactide-*co*-glycolide) scaffold supports mesenchymal stem cell differentiation and calcium phosphate deposition

Serena Casagrande, Roberto Tiribuzi, Emanuele Cassetti, Francesca Selmin, Gian Luca Gervasi, Lanfranco Barberini, Marco Freddolini, Maurizio Ricci, Aurélie Schoubben, Giuliano G. Cerulli & Paolo Blasi

To cite this article: Serena Casagrande, Roberto Tiribuzi, Emanuele Cassetti, Francesca Selmin, Gian Luca Gervasi, Lanfranco Barberini, Marco Freddolini, Maurizio Ricci, Aurélie Schoubben, Giuliano G. Cerulli & Paolo Blasi (2018) Biodegradable composite porous poly(dl-lactide-*co*-glycolide) scaffold supports mesenchymal stem cell differentiation and calcium phosphate deposition, Artificial Cells, Nanomedicine, and Biotechnology, 46:sup1, 219-229, DOI: 10.1080/21691401.2017.1417866

To link to this article: https://doi.org/10.1080/21691401.2017.1417866

ARTIFICIAL CELLS, NANOMEDICINE, AND BIOTECHNOLOGY
2018, VOL. 46, NO. S1, S219–S229
https://doi.org/10.1080/21691401.2017.1417866

Biodegradable composite porous poly(DL-lactide-*co*-glycolide) scaffold supports mesenchymal stem cell differentiation and calcium phosphate deposition

Serena Casagrande[a]*, Roberto Tiribuzi[b]*, Emanuele Cassetti[a], Francesca Selmin[c], Gian Luca Gervasi[b], Lanfranco Barberini[d], Marco Freddolini[b], Maurizio Ricci[a], Aurélie Schoubben[a], Giuliano G. Cerulli[b,e] and Paolo Blasi[f]

[a]Dipartimento di Scienze Farmaceutiche, Università degli Studi di Perugia, Perugia, Italy; [b]Laboratorio di Biologia e Medicina Rigenerativa, Istituto di Ricerca Traslazionale per l'Apparato Locomotore Nicola Cerulli-LPMRI, Arezzo, Italy; [c]Dipartimento di Scienze Farmaceutiche, Università degli Studi di Milano, Milano, Italy; [d]Dipartimento di Chimica, Biologia e Biotecnologie, Università degli Studi di Perugia, Perugia, Italy; [e]Istituto di Clinica Ortopedica e Traumatologica, Università Cattolica del Sacro Cuore-Policlinico Universitario Agostino Gemelli, Roma, Italy; [f]Scuola di Scienze del Farmaco e dei Prodotti della Salute, Università di Camerino, Camerino, Italy

ABSTRACT

In recent decades, tissue engineering strategies have been proposed for the treatment of musculoskeletal diseases and bone fractures to overcome the limitations of the traditional surgical approaches based on allografts and autografts. In this work we report the development of a composite porous poly(DL-lactide-*co*-glycolide) scaffold suitable for bone regeneration. Scaffolds were produced by thermal sintering of porous microparticles. Next, in order to improve cell adhesion to the scaffold and subsequent proliferation, the scaffolds were coated with the osteoconductive biopolymers chitosan and sodium alginate, in a process that exploited electrostatic interactions between the positively charged biopolymers and the negatively charged PLGA scaffold. The resulting scaffolds were characterized in terms of porosity, degradation rate, mechanical properties, biocompatibility and suitability for bone regeneration. They were found to have an overall porosity of ~85% and a degradation half time of ~2 weeks, considered suitable to support *de novo* bone matrix deposition from mesenchymal stem cells. Histology confirmed the ability of the scaffold to sustain adipose-derived mesenchymal stem cell adhesion, infiltration, proliferation and osteo-differentiation. Histological staining of calcium and micro-analysis confirmed the presence of calcium phosphate in the scaffold sections.

ARTICLE HISTORY
Received 11 October 2017
Revised 10 December 2017
Accepted 12 December 2017

KEYWORDS
Microparticle sintering; chitosan; alginate; bone tissue engineering; adipose-derived mesenchymal stem cells

Introduction

Tissue engineering is the third therapeutic strategy in the broad area of regenerative medicine, after the first two strategies, i.e. organ transplantation and reconstructive surgery, which have been contributing to save and improve countless lives over the years, but which nonetheless remain partial and imperfect solutions [1,2]. Tissue engineering approaches have been studied for almost all the tissues of the human body with relatively promising results [3].

Unlike other tissues, bone can regenerate itself and in most cases, bone injuries heal without scar formation, as is the case, for example, with fractured bones. Even so, bone is one of the most frequently transplanted tissues [4]. The increase of the elderly population will inevitably lead to an increasingly frail population at greater risk of bone fracture, caused not only by accidental falls, but also by diseases such as osteoarthritis and osteoporosis; this trend will place a tremendous socio-economic burden on world healthcare systems [5,6]. This may explain why the last two decades have seen growing interest in and great expectations about the possible applications of tissue engineering on bone defects.

Bone defects include bone loss after infection or cancer, bone fragility due to genetic diseases such as osteogenesis imperfecta, as well as pathological fractures such as large bone defects with delayed unions and non-unions. The traditional approaches for treating bone defects include bone allograft and autograft [7–9]. Autograft is still considered the "gold standard" for healing bone defects. It possesses all the requirements desired in a bone grafting material: it is osteoconductive (it provides a support for cell and bone tissue ingrowth), osteoinductive (it provides the differentiation of stem cells in osteogenic cells) and osteogenic (it holds viable cells for the formation of new bone tissue) [10]. However, the available volume of autologous bone graft from a patient is limited and an additional surgical procedure is required to harvest the grafting material, with a significant risk of donor site morbidity and more pain for the patient. Allograft (substitute bone obtained from a donor) is an alternative option with major limitations associated with immunological rejection, transmission of diseases and cost. Moreover, due to the

CONTACT Paolo Blasi paolo.blasi@unicam.it Scuola di Scienze del Farmaco e dei Prodotti della Salute, Università di Camerino, Camerino, Italy
*These authors equally contributed to the work.

Supplemental data for this article can be accessed here.

treatment to remove antigenicity, allografts do not contain viable cells, and thus lack osteogenicity.

Due to the limitations of the traditional grafting approaches, scientists are exploring the application of tissue engineering strategies to facilitate bone healing and regeneration [7–11]. The main focus of bone tissue engineering is the creation of an appropriate scaffold, which acts as a three-dimensional support to guide *de novo* tissue formation. Scaffolds must be biocompatible, and their surface features must be such that they assure cell adhesion and attachment [12]. They must have high porosity to allow cell migration and proliferation and facilitate the transport of nutrients [13], and their mechanical properties must match those of the tissue. Similarly, their degradation rate must be in line with the tissue regeneration kinetics [7,14].

In the current study, three-dimensional biodegradable scaffolds were designed by sintering together poly(DL-lactide-*co*-glycolide) (PLGA) porous microparticles (MPs) with tailored porosity and size. To improve the scaffold-cell interaction, its surface was coated with chitosan (CH) and alginate (AL), biopolymers that have demonstrated osteoconductive properties [15,16]. The scaffolds were characterized in terms of morphology, porosity, degradation rate, mechanical behaviour and *in vivo* biocompatibility. Then, we investigated the ability of this construct to support adipose-derived mesenchymal stem cells (AD-MSCs) adhesion and differentiation as well as the possibility of obtaining *de novo* bone matrix by calcium phosphate deposition. This study reports the feasibility of a biocompatible and biodegradable scaffold that can support mesenchymal stem cell differentiation to bone and promote significant calcium phosphate deposition.

Materials and methods

Materials

PLGA Resomer® 502 H ($M_w \sim 8000$ Da), with a 50:50 ratio of lactic:glycolic acids, was supplied by Boehringer Ingelheim (Ingelheim, Germany) and used as provided. Polyvinyl alcohol (PVA) (M_w: 30,000–70,000 Da), chondroitin-4-sulphate sodium salt (CS) from bovine trachea, sorbitan monostearate (Span® 60), polysorbate 80 (Tween® 80) and sodium azide were purchased from Sigma-Aldrich (Milan, Italy). High mannuronic sodium alginate (guluronic acid, 39%; mannuronic acid 61%) and low molecular weight CH (Mw ~150,000 Da) were supplied by Stern (Milan, Italy) and Fluka (Milan, Italy), respectively.

Fertilized eggs used for chicken embryo chorioallantoic membrane (CAM) assay were supplied by Azienda Agricola Cerquaglia (Marsciano, Italy). Mayer's haematoxylin, eosin and alizarin red employed for histology staining were purchased from Carlo Erba (Milan, Italy). Type I collagenase, Dulbecco's Modified Eagle's medium (DMEM) and foetal bovine serum (FBS) were supplied by Sigma-Aldrich (Milan, Italy), while the commercial osteogenic induction medium Poietics™ was purchased from Lonza (Walkersville, MD, USA). All antibodies (Abs) employed for flow cytometry were purchased from Becton Dickinson (Frankin Lakes, NJ, USA), except for the PE-conjugated anti-human CD73, supplied by Miltenyi Biotech (Bologna, Italy). All FACS reagents were used in the concentrations recommended by the manufacturer.

Ultra-pure water was obtained from a New Human Power system (Human Corporation, Seoul, Korea). All other chemicals were of the highest purity commercially available and used as provided.

Microparticle preparation and characterization

Porous PLGA MPs were prepared according to a water-in-oil-in-water (W/O/W) double emulsion method [17]. After an initial method optimization (Table S1), optimal MPs were obtained using the following parameters: 1.5 ml of 0.1% (w/v) Span® 60 were emulsified in 3.5 ml of CH_2Cl_2 containing 500 mg of PLGA (W_1/O). This primary emulsion was slowly injected into 500 ml of 0.1% w/v PVA solution (W_2) forming a W_1/O/W_2 emulsion that was stirred at 600 rpm until complete organic solvent evaporation. The injection was performed at 4 °C, then the temperature was increased to 25 °C, maintained at 25 °C for 2 h, raised up to 30 °C for 1 h, and 40 °C for 30 min. The accuracy of the temperature controller was ±1 °C. After the MP formation and hardening, the temperature was lowered to 15 °C and the dispersion was filtered using a cellulose filter having a pore size of 2.5 μm (Whatman®, Maidstone, UK), washed three times with ultrapure water. MPs were dried at room temperature overnight and for an additional 12 h under vacuum.

Microparticle mean diameter and size distribution were estimated with an Accusizer C770 (PSS Inc. Santa Barbara, USA) equipped with an autodiluting system (Autodiluter™, PSS Inc. Santa Barbara, CA, USA). Dried MPs were suspended in 1 ml of ultrapure water containing 0.5% (w/v) of polysorbate 80 to prevent MP aggregation. Analyses were performed in triplicate and size was expressed as mean volume diameter (d_{mv}) ± standard deviation.

Microparticle morphology was investigated by scanning electron microscopy (SEM) using a Philips XL30 microscope (Philips Electron Optics, Eindhoven, Netherlands). Samples were prepared by placing a small amount of MPs onto an aluminium specimen stub. The samples were sputter coated with gold prior to imaging (EMITECH K-550X sputter coater Ashford, Kent, UK). Coating was performed at 35 mA for 3 min.

Scaffold preparation and characterization

Scaffolds were prepared using the thermal sintering technique [18]. PLGA MPs were placed in a cylindrical mould (diameter: 7 mm; depth: 5 mm) and incubated at different temperatures and times to identify the optimal conditions for obtaining scaffolds with the desired characteristics. The optimized scaffold was prepared sintering 200 mg of MPs at 60 ± 2 °C for 1 h. The scaffold was then coated with CH and AL [19,20]. Briefly, the scaffold was dipped in 5 ml of a 1% (w/v) CH solution for 15 min, then in 5 ml of a 1% (w/v) AL solution for 15 min, washed in 5 ml of distilled water for 15 min and finally lyophilized using a Virtis Benchtop Freeze Dryer 8 l 105 C (Ipswich, UK) at −80 °C

and 158 mtor of temperature and pressure, respectively. Hereafter, the CH and AL coated scaffold is referred to as 'coated scaffold', while the bare scaffold is referred to as "uncoated scaffold".

To assess the efficacy of the coating procedure, scaffolds were also coated with CS instead of AL and the presence of the external polyanion was detected by microanalysis using a Philips XL30 SEM (Philips Electron Optics, Eindhoven, Netherlands) coupled with an EDAX Philips system equipped with an LaB6 source and an EDAX/DX4 detector. Scaffolds were sputter coated with gold prior to imaging (EMITECH K-550X sputter coater Ashford, Kent, UK). Coating was performed at 35 mA for 3 min.

Scaffold surfaces were also analysed by Attenuated Total Reflection-Fourier Transform Infrared Spectroscopy (ATR-FTIR) (Fourier Nicolet AVATAR 360 N equipped with a Nicolet Smart DuraScope sensor, a video-enhanced diamond ATR and an integrated camera). The operating parameters were the following: sampled area, 1.5 mm^2; sampled volume, 2 μL; penetration, 2 μm; number of scan, 64.

Scaffold porosity was estimated using computed tomography (CT) scans performed by a Vimago™ CT Scanner (Epica Medical Innovations, San Clemente, CA, USA) with a resolution of 100 μm and true isotropic voxels. Scans were done with an energy level of 65 kV, an exposure time of 5 ms and an X-ray tube current of 25 mA. Image slices were acquired with a thickness and a pixel size of 90 μm.

Computed tomography image segmentation was performed using open access MicroDicom software; a region of interest (ROI) of 8×8 mm was chosen for each slice and a threshold was used to create a black/white image of the slice. The percentage of white pixels relative to the total number of pixels of the ROI was estimated using a custom-made script within MATLAB (The MathWorks, Inc., Natick, MA, USA) for each slice. Then, porosity was calculated as the mean of the percentage of white pixels relative to the total number of pixels for each slice. The results were expressed as the mean of three independent measurements for both uncoated and coated scaffolds.

Scaffold degradation

Scaffold degradation was evaluated by *in vitro* mass loss studies and gel permeation chromatography (GPC).

Scaffolds were inserted in a closed tea bag built with a polyester net (pore diameter 30 μm) and incubated in 40 ml of phosphate-buffered saline (PBS) (0.1 M, pH 7.4) containing 0.02% (w/v) of sodium azide at 37 °C. Scaffolds were withdrawn after 1 h (T0) and 1 (T1), 7 (T7), 14 (T14), 21 (T21) and 28 (T28) days, washed with 50 ml of ultrapure water, wiped with filter paper and vacuum dried overnight. The analysis was performed in triplicate and the error was expressed as standard deviation.

Mass loss (ML) and residual mass (RM) were calculated as follows

$$\mathrm{ML}(\%) = \frac{\text{Initial mass} - \text{Mass recovered after incubation}}{\text{Initial mass}} \times 100 \quad (1)$$

$$\mathrm{RM}(\%) = \frac{\text{Mass recovered after incubation}}{\text{Initial mass}} \times 100 \quad (2)$$

Polymer molecular weight (M_w) and molecular number (M_n) of the scaffolds were determined by a HP1100 Chemstation (Hewlett-Packard, Palo Alto, CA, USA) equipped with a combination of two columns: μStyragel™ Toluene 104 Å 7.8×300 mm and μStyragel™ Toluene 103 Å 7.8×300 mm (Waters, Vimodrone, Italy). The chromatographic conditions used were the following: tetrahydrofuran as a mobile phase; flow rate of 1.0 ml min^{-1}; refractive index signal as detector; injection volume of 20 μL. The M_w of each sample was calculated using a calibration curve built using monodisperse polystyrene standards with M_w ranging from 1000 to 45,000 Da.

The apparent degradation rate (K) based on M_w and M_n was obtained by:

$$\log M = \log M_0 - K \quad (3)$$

where M is the polymer M_w or M_n at time t, M_0 is the polymer M_w or M_n at time zero.

The polymer degradation half time ($t_{1/2}$) was further calculated by:

$$t_{1/2} = \log 2/K \quad (4)$$

Morphological changes during the *in vitro* degradation experiments were followed by SEM (Zeiss LEO 1525 equipped with a GEMINI column, Oberkochen, Germany). Dried scaffolds were placed on an aluminum stub by double-sided adhesive carbon tape and sputter-coated with graphite for 20 s.

Mechanical tests

Compression tests of uncoated and coated scaffolds were performed with a universal loading frame machine Instron™ 5965 (Instron Inc., Norwood, MA, USA) equipped with a 5 kN load cell on the movable part to record the compressive force during the test. The upper plate moved down at a fixed speed of 0.1 mm/s, compressing the scaffold against the lower plate until reaching half of the initial thickness. Dried scaffolds and scaffolds incubated in PBS (0.1 M, pH= 7.4, with 0.02% w/v of sodium azide) at 37 ± 1 °C and withdrawn at 1 h (T0) and 1 (T1), 7 (T7), 14 (T14), 21 (T21) and 28 (T28) days were tested. Scaffold dimensions were assumed equal to compare data of compression tests (5 mm of thickness and 15 mm of width). The Young's modulus was calculated as the ratio between compressive stress and strain in the linear portion of the curve. Tests were executed using four scaffolds for each group and results were expressed as mean ± standard deviation. Statistical analysis was performed using MATLAB software (The MathWorks, Inc., Natick, MA, USA). Comparison between uncoated and coated scaffolds was done by student t-test and the difference was considered to be statistically significant if $p < .05$.

In vivo biocompatibility studies

Chorioallantoic membrane assay was performed to evaluate the *in vivo* biocompatibility of coated and uncoated scaffolds [21]. Fertilized eggs were incubated at 38 ± 1 °C and 60% of relative humidity in a ventilated non rocking oven. On day 3, an opening with a diameter of about 3 cm was made on the obtuse pole of the eggshell and viable embryos were selected for the experiment. The eggshell window was closed with a polyethylene film to avoid water loss and microbial contamination. Four days later (day 7 of development), uncoated and coated scaffolds were deposited on the CAM surface. Embryos were monitored for macroscopic signs of toxicity and photographed every day until day 12 of development [22,23]. Embryos were sacrificed at day 12 and the portions of CAM with the scaffolds were sampled and fixed in 4% (w/v) paraformaldehyde in PBS (pH 7.4). Samples were dehydrated in ethanol solutions of growing order of gradation (from 70 to 100°), treated in xylol and then embedded in paraffin. Each sample was cut with a rotary microtome (RM 2145 Leica Microsystems, Nussloch, Germany) into 10 μm slides (orthogonal section) that were treated with xylol to eliminate the paraffin and then with ethanol (decreasing order of gradation) to allow the staining. CAM was stained with Mayer's haematoxylin solution and eosin. After staining, the slides were again dehydrated and mounted with coverslip in Canada balsam before histological examination, performed with a Leica DMLB light microscope (Wetzlar, Germany), equipped with a Leica DFC 320 high-resolution camera.

Isolation and characterization of adipose-derived mesenchymal stem cell

Tissue isolation

Infra-patellar fat-pat-biopsies were isolated from patients undergoing total knee arthroplasty at the International Orthopedic and Traumatologic Institute (IOTI) (Arezzo, Italy), following a standardized protocol meeting the criteria established by the American College of Rheumatology [24]. At the beginning of the surgical procedures, infra-patellar fat pad biopsies were collected and sent to IRTAL-LPMRI (Istituto di Ricerca Traslazionale per l'Apparato Locomotore Nicola Cerulli – Lpmri – S.r.l.) within 4 h.

Isolation of adipose-derived mesenchymal stem cells

Fat tissue biopsies were processed to obtain AD-MSCs. Briefly, fat biopsies were washed extensively with sterile PBS supplemented with 5X antibiotics (500 U/ml Pen/Strep) and treated with 0.075% collagenase type I in PBS for 30 min at 37 ± 1 °C under gentle agitation. Collagenase was inactivated with an equal volume of DMEM/10% FBS and the infranatant was filtered through a 70-μm mesh filter to remove tissue debris, and then centrifuged (10 min at 200*g*). The cellular pellet was resuspended in DMEM/10% FBS, plated onto conventional tissue culture plates in normal growth medium (NGM: DMEM low glucose +10% FBS +100 U/ml Pen/Strep), and expanded until the third passage, after which they were used for the experimental procedures.

Flow cytometry

Adipose-derived mesenchymal stem cells were cultured in control medium for 72 h before analysis. Cells were harvested in 0.25% trypsin/EDTA and washed three times in an isotonic phosphate buffer (supplemented with 0.5% BSA). Washed cells were re-suspended in PBS containing 0.5% FBS at a final concentration of 1×10^6 cells/mL. All procedures were performed at 4 °C. The following Abs were used: FITC-labelled rabbit anti-human CD90, CD105, CD271 and HLA-DR; PE-conjugated anti-human CD73, FITC–conjugated anti-CD14 mAb (Leu M3) and PE-conjugated anti-CD16 mAb (Leu11). Flow cytometry data acquisition was performed on a FACS Calibur equipped with 488 and 633 nm lasers and running Cellquest Software (Becton Dickinson, CA, USA). Ten thousand live-gated events were collected for each sample and isotype matched Abs were used to determine binding specificity. The results were expressed both as a percentage of positive cells/antibody used for staining (% positive cells) and as mean fluorescence intensity (MFI).

AD-MSCs growth and osteogenic differentiation

AD-MSCs (total number 2.5×10^5) were seeded on coated scaffolds in presence of the normal growth medium (NGM) and cultured for 24 h. Afterwards, the AD-MSC osteogenic differentiation was induced, replacing the NGM with a commercial osteogenic differentiation medium containing dexamethasone, L-glutamine, ascorbate, mesenchymal cell growth supplement, β-glycerophosphate, penicillin/streptomycin, complemented following manufacturer instructions. As experimental control, AD-MSCs were seeded in coated scaffolds and cultured only in the NGM. The culture medium was changed every three days and cells were maintained in culture for 60 days. After selected time points (3, 7, 21, 35 and 60 days of culture), scaffolds were harvested and washed with sterile PBS. Cells were fixed using PBS containing 4% (w/v) of paraformeldehyde and 1% (w/v) of glutaraldehyde.

Fixed scaffolds were washed with ultrapure water, embedded in optimum cutting temperature (OCT) compound and frozen at -20 ± 1 °C. Sixteen μm scaffold sections were prepared using a Cryostat microtome. Cell proliferation and penetration into scaffolds were evaluated by Haematoxylin–Eosin (HE) staining. Briefly, scaffold sections were incubated in Mayer's haematoxylin solution for 15 min at room temperature, washed with water and stained with eosin solution for 5 min at room temperature. Samples were dehydrated in ethanol solutions of growing order of gradation (from 70° to 100°). To assess calcium deposition, scaffolds were stained using 2% (w/v) alizarin red for 5 min at room temperature. Sections were dehydrated in ethanol (from 70° to 100°). All scaffold sections stained were evaluated under a Leica DMLB light microscope equipped with a Leica DFC 320 high-resolution camera.

The scaffold sections were deposited on glass slides and sputter-coated with graphite for 20 s to collect SEM images and perform elemental mapping with energy dispersive X-ray spectroscopy (EDS).

Results

Scaffold preparation and characterization

Optimized PLGA MPs obtained with the solvent evaporation technique had a particle size (d_{mv}) in the range of 150–200 μm, suitable for preparing sintered scaffolds for tissue regeneration (Figure 1(a,b)) [25]. The use of the double emulsion preparation method made it possible to obtain MPs with the high internal porosity required to assure fast degradation and increasing porosity over time (Figure 1(c)).

The scaffold preparation was performed using thermal sintering. Incubation temperature and holding time were optimized to guarantee the transition from the glassy to the rubbery state of PLGA (PLGA $T_g \sim 38\,^{\circ}C$) and the fusion of MPs in direct contact. Scaffolds that were easy to handle without failure or loss of materials and that had a highly interconnected pore structure were prepared by sintering 200 mg of MPs at 60 °C for 1 h.

Next, scaffolds were coated with CH and AL. Preliminarily, CS and CH were used as model polymers to assess the suitability of the experimental protocol to provide a uniform coating layer on the scaffolds. Microanalysis spectra evidenced the presence of sulphur, attributed to the CS sulphate groups only on the coating (Figure 1(d)), while the signal was not measured in the scaffold cross section (Figure 1(e)). The presence of the coating was also confirmed by ATR-FTIR analysis. Spectra of the PLGA, CH, CS alone and of the scaffold coated with CH and CS were acquired. The spectrum of the pure PLGA showed a sharp and high intensity peak at 1751 cm^{-1}, ascribed to the C = O stretching of the ester group [26]. CS spectrum showed a broad absorption in the region of the –OH and –NH stretching modes (3000–3650 cm^{-1}), ascribed to the hydroxyl and amino groups present in the backbone, and two medium intensity bands at 1608 and 1558 cm^{-1}, due to the C = O stretching and NH–CO bending vibration, respectively (Figure S1a). In the CH spectrum, the same bands present in the CS spectrum were observed, but at slightly different wavelengths: the C = O stretching and the NH–CO bending peaks were situated at 1647 and 1558 cm^{-1}. In the scaffold coated with CH and CS, a broad band in the range of 3000–3600 cm^{-1} and two peaks at 1628 and 1539 cm^{-1} were recorded. The intensity of the last two peaks were equivalent to the sum of the intensity of the corresponding peaks of the single biopolymers, confirming the CH and CS contribution (Figure S1b). In addition, a low intensity peak at 1743 cm^{-1} was observed in the coated scaffold spectrum, probably ascribable to the C = O stretching of PLGA under the coating layer (Figure S1a). The shift to lower frequencies of the peaks of the single polymers in comparison to those observed in the scaffold spectrum suggests the formation of intermolecular interactions between the polymers [27].

Scaffold degradation

In vitro mass loss studies showed a biphasic profile for both the uncoated and coated scaffolds [28]. The first week was characterized by low mass loss, while faster mass loss occurred during the following weeks (Figure 2(a)). In the second phase (from T7 to T28), the mass loss rate was comparable for both scaffolds (−3.0184 day^{-1} for the uncoated

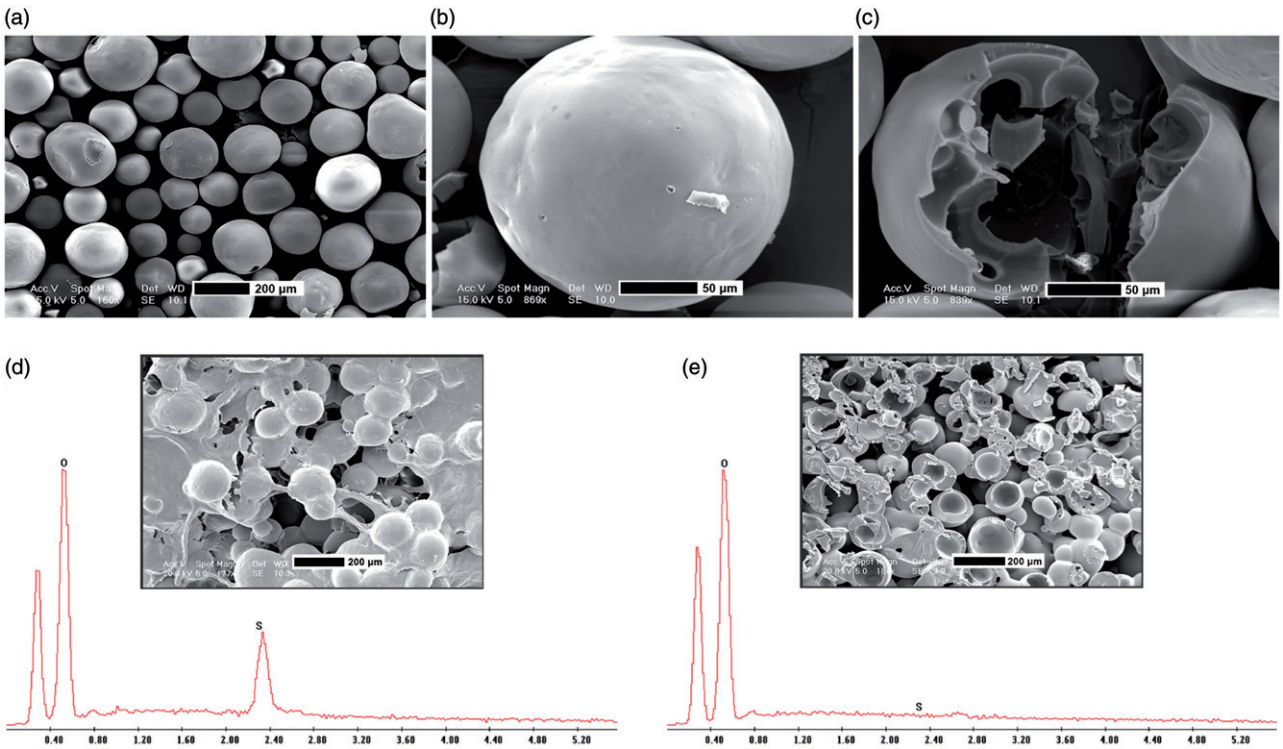

Figure 1. SEM micrographs of PLGA microparticles, prepared using the solvent diffusion/evaporation method, at different magnification (a, b). Panel c of the cut microparticle shows the inner particle porosity. Microanalysis spectra of the upper surface (d) and of the cross section (e) of the scaffold coated with chitosan/chondroitin-4-sulphate. The inserts show SEM micrographs of the scaffold upper surface (d) and cross section (e).

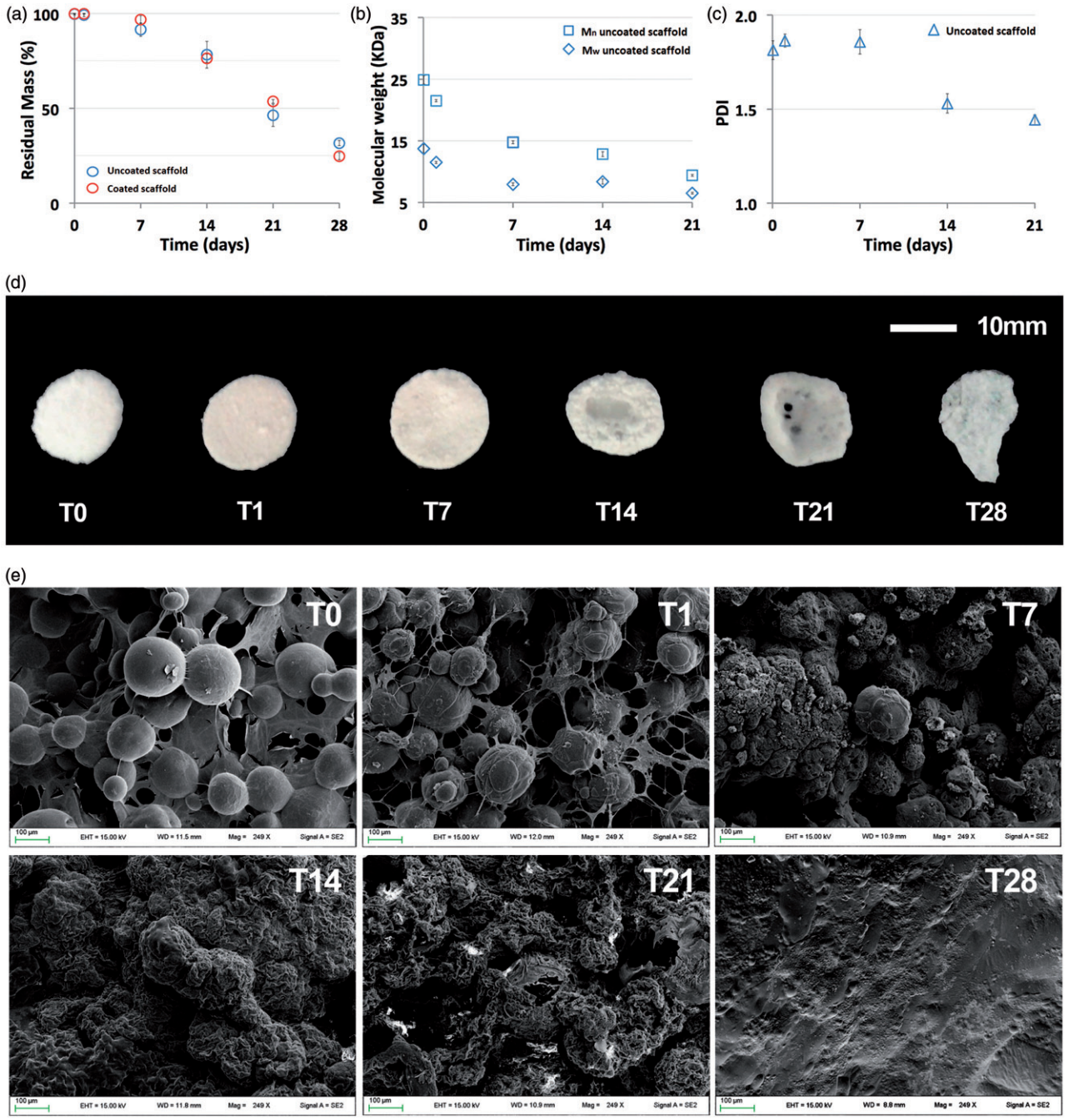

Figure 2. Comparison of the residual mass between uncoated and coated scaffolds over the 28 days of the degradation period (a). Polymer M_w (b), M_n (b) and PDI (c) profile of uncoated scaffolds during degradation. Photos of coated scaffolds at 1 h (T0), and 1 (T1), 7 (T7), 14 (T14) and 21 (T21) days of degradation in PBS (0.1 M, pH 7.4) at 37 °C (d). SEM micrographs of the upper surface of the coated scaffold at different degradation times (e).

scaffold and −3.4131 day^{-1} for the coated one) and at 28 days, the residual mass was around 25% (Figure S2).

Scaffold degradation was also evaluated by GPC. First of all, M_w of pure PLGA and MP were compared. The thermal sintering technique did not significantly impact the polymer M_w and polydispersity index (PDI). After the MP sintering procedure to obtain the scaffolds, a slight decrease in polymer M_w (about 2%) was measured along with a variation in PDI from 1.80 to 1.76 (data not shown).

The *in vitro* polymer hydrolysis of uncoated scaffolds was studied at pH 7.4 in PBS for 21 days. Both M_n and M_w of scaffolds decreased exponentially with time throughout the degradation period, according to the typically exponential decay reported for this class of polymers (Figure 2(b)) [29]. Data points were normalized considering polymer M_w and M_n of the scaffolds incubated 1 h in PBS as 100%. The apparent degradation rates based on M_w and M_n calculated using Eq. (3), were estimated to be 0.0188 and 0.0133 week^{-1}, respectively. Degradation half times derived from M_w (Eq. (4)) were about 2.3 weeks. Polymer M_w distribution exhibited the expected single peak. As the scaffolds degraded and low molecular weight polymers were produced, the peak broadened and shifted to the right, sometimes along with a small shoulder. These features were in agreement with the changes in PDI, which remained almost constant for about 10 days until a significant decrease of M_w took place (Figure 2(c)).

In the case of coated scaffolds, the accuracy of GPC analysis was compromised, probably by the presence of residual CH coating that could not be completely removed. Indeed, ATR-FTIR data confirmed the presence of an interaction between the PLGA scaffold and the coating. It can be assumed that CH chains, which are positively charged, can form electrostatic interactions with the PLGA negatively charged surface. This feature is in agreement with the model proposed by Guo and Gemeinhart. The adsorption of chitosan follows a multilayer adsorption behaviour suggesting that the adsorption of chitosan occurred on an energetically heterogeneous surface. Chemical heterogeneity (the distribution of carboxylic end group and intermediate segments of PLGA molecules) could also contribute to this interaction [30].

Scaffold morphology and structure were affected by the biphasic degradation behaviour. Changes in size and surface morphology of coated scaffolds are shown in Figure 2(d). In the first stage of degradation (until T7), scaffold dimensions basically remained unchanged, while in the late stage of degradation, the scaffold surface gradually became irregular. As reported in other works, the scaffold dimensions slightly increased just before decreasing dramatically [31]. The same behaviour was observed for uncoated scaffolds (data not show). The SEM micrographs were in agreement with the results of degradation studies. From hydration time T7, the scaffold surface became irregular and rough, and MPs started to lose their spherical shape. Interestingly, at T21, pores and the interconnected structure were still visible (Figure 2(e)).

Mechanical test

PLGA is basically an elastic-plastic material, and in fact, the pattern of slope did not show a precise yielding point. Normally this event is more visible with low porosity [32], but in our study the porosity, estimated from CT scans (Figure 3(a)), was higher than 85%, so the yielding peak vanished from the curve. First, mechanical properties were evaluated for dried scaffolds. In particular, average maximum compressive stress was significantly higher (1.151 ± 0.058 MPa) for uncoated scaffolds when compared with the coated ones (0.478 ± 0.005 MPa). Young's modulus for dry scaffolds was also compared between uncoated and coated groups at 50% and 75% of strain. Uncoated scaffolds showed a higher Young's Modulus at all strains (0.314 ± 0.095 MPa vs 0.278 ± 0.076 MPa at 50%; 0.949 ± 0.038 MPa vs 0.526 ± 0.077 MPa at 75% for uncoated vs coated scaffolds). The difference was significant ($p < .05$) at 75% of strain.

Mechanical properties were then evaluated at five different hydration times in PBS (0.1 M, pH 7.4, 37 °C): T0, T1, T7, T14,

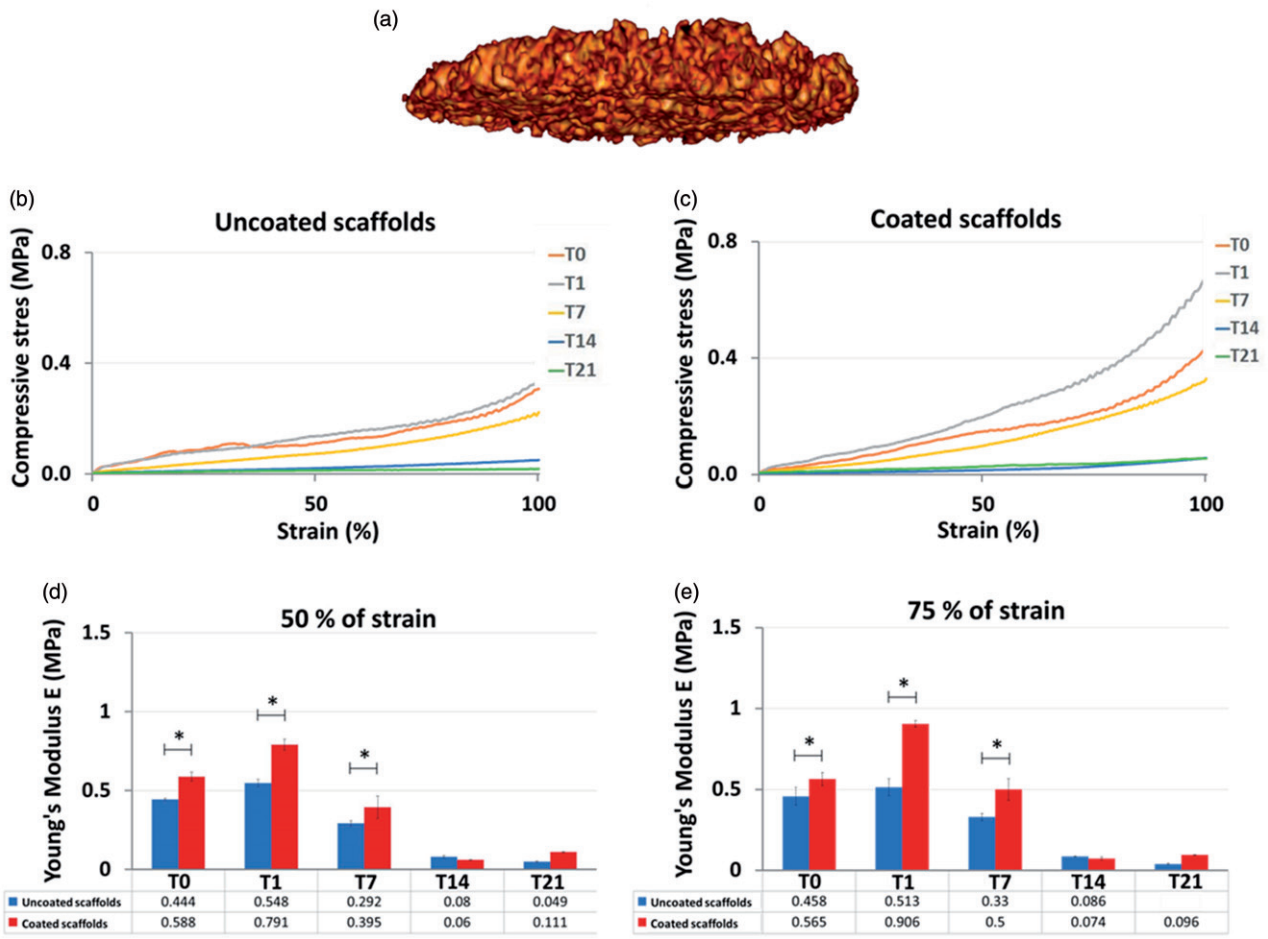

Figure 3. Coated scaffold rendering of computed tomographic (CT) images (a). Compressive stress of uncoated (b) and coated (c) scaffolds and the Young's modulus at 50% (d) and 75% (e) of strain for the scaffolds after 1 h (T0) and 1 (T1), 7 (T7), 14 (T14) and 21 (T21) days of incubation in PBS (0.1 M, pH 7.4) at 37 °C. Data are expressed as mean ± SD, $^{*}p < .05$ by student *t*-test.

and T21 (1 h and 1, 7, 14, 21 days of hydration, respectively). In Figure 3, results of uncoated (b) and coated (c) scaffolds are shown as stress-strain curve slope, where stress was calculated as the force per unit area and strain as the normalized deformation induced in percentage. Significant differences in compressive resistance were found at T0, T1 and T7 hydration time. Low compressive stress after 14 days of hydration (T14) was not representative because the scaffolds were subjected to considerable degradation, which drastically reduced their mechanical properties. Figure 3(d,e) shows Young's modulus at 50% and 75% of strain. Differences between uncoated and coated scaffolds were all statistically significant ($p < .05$) for T0, T1 and T7. Young's modulus tended to increase from T0 to T1, then it decreased due to the scaffold degradation.

In vivo biocompatibility

Chorioallantoic membrane assay showed high biocompatibility of both uncoated and coated scaffolds. Digital images captured five days after the deposition of coated scaffolds on CAM surface showed a normal vascular growth without adverse reactions or inflammation, generally recognized as bleeding, ghost vessels and neoangiogenesis, around the scaffold (Figure 4(a)). The absence of adverse reactions was also confirmed by observing the CAM under the scaffolds after sampling for histology (data not shown). Histological examination confirmed the absence of toxicity and revealed just a slight thinning of the CAM due to the scaffold weight [33,34]. CAM had a normal histology without modification of the ectoderm, mesoderm, or endoderm. Nucleated red blood cells were normal as well. Of note, the coated scaffold showed important and deep cell invasion, as evident in Figure 4(b,c). Cells were found not only in the biopolymer in direct contact with the biological substrate but also in the scaffold porosity (Figure 4(c)). By a combination of capillarity and biopolymer cell adhesion, cells penetrated the 3 D structure of the scaffold deeper than 0.5 mm. The scaffold acted on CAM like a tissue graft [35]. The presence of the scaffold on the CAM caused localized hypertrophy of the membrane that reached more than 1 mm thickness. In addition, the ectoderm in contact with the scaffold manifested the classical reaction due to tissue fragment implantation. Ectoderm cells started to proliferate very rapidly (presence of numerous mitoses and multinuclear cells) and to invade the tridimensional structure.

AD-MSCs immunophenotype

The surface marker expression of cultured AD-MSCs cells was analysed using flow cytometry. The majority of the cells were positive for CD73 (97.5 ± 2.12%), CD90 (89.5 ± 7.78%), CD105 (90 ± 9.89%) and negative for HLA-DR, CD271, CD14 and CD16 (values <1%). These data indicated that the cells had the mesenchymal-specific surface antigen pattern [36].

Osteogenic differentiation of AD-MSCs

AD-MSCs seeded onto coated scaffolds attached and adhered to the surface first, but histological analysis (HE staining) showed a gradual cell invasion and penetration into the polymer matrix over time. At seven days from seeding, AD-MSCs were mainly located on the scaffold surface, while, at 60 days, cells proliferated and invaded the internal scaffold matrix (Figure 5(a–d)). Over time, HE stained cells changed from pink-red to blue, confirming a higher metabolic activity and proliferation [37]. To evaluate calcium deposition and the matrix mineralization, scaffold sections were also stained with AR. Results showed no red staining in scaffolds harvested at 7 and 23 days (data not shown). Small calcium deposits were present at day 35 while, at day 60, slices showed intense and uniform red staining, which suggests that at 60 days of culture, the already degraded polymer matrix was mainly replaced by mineralized bone matrix, composed essentially of calcium phosphate salts (Figure 5(e–f′)). To confirm the presence of calcium phosphate, microanalysis was performed. EDS data showed the presence of both Ca and P that co-localize in the histological sections (Figure 5(g-g‴)).

Discussion

PLGA is one of the most studied polymers in tissue engineering because of its high biocompatibility, tailored biodegradability and suitable mechanical properties [14,32]. In this study, we used PLGA sintered MPs to build 3 D scaffolds suitable for bone regeneration. Among the different methods reported in literature, thermal sintering shows several advantages. It allows the preparation of 3 D scaffolds with high inner interconnectivity and a tailored pore size, without the

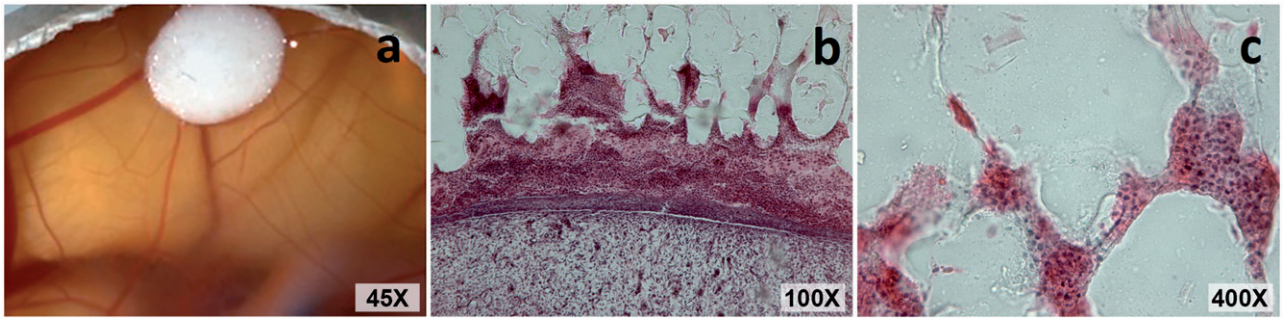

Figure 4. CAM assay of the coated scaffold (a). Histology of the scaffold deposed on the CAM at 100× magnification (b) and 400× magnification (c). Scaffold sections were stained with hematoxylin and eosin.

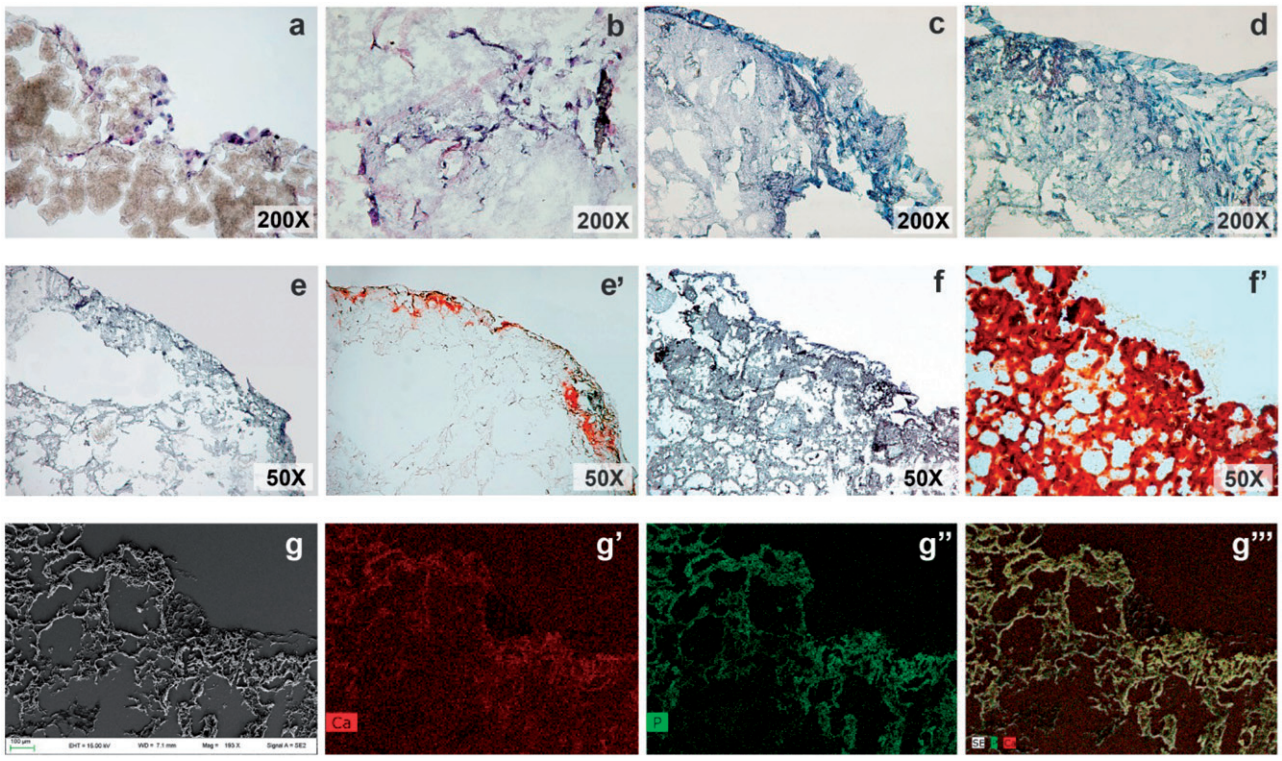

Figure 5. Cross section (16 μm) of the coated scaffolds at 7 (a), 23 (b), 35 (c) and 60 (d) days of culture in a commercial osteogenic differentiation medium (Lonza™). Sections were stained with HE staining methods. Comparison between scaffold sections stained with HE and AR at 35 (e, e′) and 60 (f, f′) days of culture in the induction medium. Calcium deposits are stained in red (e′, f′). SEM micrograph (g) and microanalysis of a section of the scaffold at 60 days of culture in induction medium. Ca mapping (g′), P mapping (g″) and overlapping image (g‴).

use of porosigen agents, overcoming some drawbacks of phase separation, gas foaming, and salt leaching techniques [38]. In addition, particle sintering offers high surface area for cell adhesion and expansion compared to that of other methodologies. High porosity is an essential requirement for tissue engineering applications, as it facilitates cell diffusion and migration, ECM deposition and vessel penetration. A porous surface also improves the integration between the implanted scaffold and the surrounding tissue *in vivo* [39]. In the specific case of bone regeneration, the scaffold porosity requirement is even more important and it is essential to mimic, as much as possible, the natural bone structure. Since human trabecular bone has a variable porosity that ranges between 50 and 90% of the bone volume [40], our scaffold is adequate to reproduce the empty spaces of normal bone tissue.

However, PLGA and related polymers do not possess adequate surface properties for cell adhesion and the use of additional materials is needed. CH and AL are natural biopolymers that have been largely exploited in tissue engineering because of their osteoconductive properties [15,16,41]. Our data showed that a coating made of a combination of these polymers creates a cell-friendly environment, and the simple scaffold deposition on intact chicken CAM was sufficient to allow cell invasion and penetration in the 3 D structure (Figure 4).

A biodegradable scaffold must be able to maintain its physical, chemical and mechanical properties until seeded cells adapt to the environment and excrete sufficient amounts of ECM. After the scaffold accomplishes its mission, it has to be completely degraded and absorbed by the body [14]. Polymer M_w was chosen to obtain a scaffold with fast degradation, so that it can be replaced by ECM and mineralized bone. It is important to point out that despite the fast degradation rate, the scaffold residual mass was around 50% after 21 days of incubation. Degradation studies data revealed biphasic behaviour, which is to be expected for polyesters that degrade via bulk degradation mechanism, and indicated that there was low mass loss during the first week and faster mass loss during the following weeks (Figure 2(a)). Conspicuous mass loss does not start until the polymer chains are reduced to a molecular weight that allows them to solubilize and freely diffuse out of the matrix [14,42].

The degradation behaviour observed in our scaffolds fits with the requirements for mesenchymal stem cell (MSC) differentiation and osteogenesis. In fact, MSC osteogenesis and osteoprogenitor differentiation can usually be divided into different stages *in vitro*. Cell proliferation occurs during the first four days, followed by an early differentiation from days 5 to 14. The final stage, from days 14 to 28, is characterized by cell maturation and deposition of a mineralized matrix [43,44]. In our study, at 21 days, the PLGA scaffold still possesses the adequate integrity and structure to provide 3 D support for cell maturation and matrix deposition.

In the current study, AD-MSCs were seeded on coated scaffolds to verify their ability to support cell osteodifferentiation and *in vitro* bone matrix deposition [45]. Histology confirmed that the scaffold supported cell adhesion, migration, proliferation and differentiation. Our results showed the first calcium deposits at 35 days, while intense and uniform red staining was reached after 60 days (Figure 5(e′,f′)). Matrix

mineralization is one of the most important indicators of *in vitro* osteogenesis and of osteogenic differentiation of MSCs. The temporal delay observed in matrix deposition, compared to that reported in previous studies [43,44], can be ascribed to the small number of cells seeded in relation to the high void volume that characterized our scaffold. However, the histology and microanalysis indicated that the biodegradable scaffold was mainly replaced by mineralized bone matrix.

Conclusions

In this work, we prepared a composite PLGA scaffold suitable for tissue engineering applications, in particular for bone tissue regeneration. Scaffold characterization showed that the sintering method seems to be a valid alternative to other methods found in the literature to produce scaffolds. Our sintered scaffolds possessed the porosity desired for bone tissue regeneration. Scaffold coating with natural biopolymers (CH and AL) improved scaffold mechanical properties as well as cell adhesion and infiltration. The degradation rate, with a residual mass of ~50% at 21 days of degradation, demonstrated the ability of the scaffold to support and sustain seeded mesenchymal stem cells until their differentiation, which occurred after approximately 21 days of culture. Histological analysis confirmed that coated scaffolds were osteoconductive and good candidates to sustain AD-MSC adhesion, infiltration and osteogenic differentiation in presence of an induction medium. According to degradation time and mechanical performance, this kind of scaffold could find application in the healing of small defects in bones that may not support high load or high mechanical stress.

Acknowledgements

The authors are indebted to Dr. Luca Poletti from Sereco Biotest www.serecobiotest.it for the ATR-FTIR analyses. They would like to express their gratitude to the LUNA (Laboratorio Universitario di Nanomateriali) laboratory of the University of Perugia and in particular to Dr. Alessandro Di Michele for SEM analysis and microanalysis. They would also like to thank Sheila Beatty for editing the English usage in the manuscript.

Disclosure statement

No potential conflict of interest was reported by the authors.

References

[1] Tabata Y. Recent progress in tissue engineering. Drug Discov Today. 2001;6:483–487.
[2] Langer R, Vacanti JP. Tissue engineering. Science. 1993;260:920–926.
[3] Lanza R, Vacanti R, Vacanti JP. Principle of tissue engineering. 4th ed. New York (NY): Elsevier Inc.; 2013.
[4] Shegarfi H, Reikeras O. Review article: bone transplantation and immune response. J Orthop Surg (Hong Kong). 2009;17:206–211.
[5] The World Bank. Population projections; 2011. [Internet] Available from: http://web.worldbank.org.
[6] Hoy D, Geere J-A, Davatchi F, et al. A time for action: opportunities for preventing the growing burden and disability from musculoskeletal conditions in low- and middle income countries. Best Pract Res Cl Rh. 2014;28:377–393.
[7] Oryan A, Alidadi S, Moshiri A, et al. Bone regenerative medicine: classic options, novel strategies, and future directions. J Orthop Surg Res. 2014;9:18–45.
[8] Henkel J, Woodruff MA, Epari DR, et al. Bone regeneration based on tissue engineering conceptions - a 21st century perspective. Bone Res. 2013;3:216–248.
[9] Giannoudis PV, Dinopoulos H, Tsiridis E. Bone substitutes: an update. Injury 2005;36S:S20–S27.
[10] Albrektsson T, Johansson C. Osteoinduction, osteoconduction and osseointegration. Eur Spine J. 2001;10:S96–S101.
[11] Vural AC, Odabas S, Korkusuz P, et al. Cranial bone regeneration via BMP-2 encoding mesenchymal stem cells. Artif Cells Nanomed Biotechnol. 2017;45:544–550.
[12] Chang H-I, Wong Y. Cell responses to surface and architecture of tissue engineering. In: Eberli D, editor. Scaffolds regenerative medicine and tissue engineering – cells and biomaterials. Croatia: In Tech d.o.o.; 2011.
[13] Karageorgiou V, Kaplan D. Porosity of 3D biomaterial scaffolds and osteogenesis. Biomaterials. 2005;26:5474–5491.
[14] Hutmacher DW. Scaffolds in tissue engineering bone and cartilage. Biomaterials. 2000;21:2529–2543.
[15] Di Martino A, Sittingerc M, Risbud MV. Chitosan: a versatile biopolymer for orthopaedic tissue-engineering. Biomaterials. 2005;26:5983–5990.
[16] Rowley JA, Madlambayan G, Mooney DJ. Alginate hydrogels as synthetic extracellular matrix materials. Biomaterials. 1999;20:45–53.
[17] Giovagnoli S, Blasi P, Schoubben A, et al. Preparation of large porous biodegradable microspheres by using a simple double-emulsion method for capreomycin sulfate pulmonary delivery. Int J Pharm. 2007;333:103–111.
[18] German RM. Sintering theory and practice. New York (NY): John Wiley and Sons; 1996.
[19] Bertland P, Jonas A, Laschewsky A, et al. Ultrathin polymer coatings by complexation of polyelectrolytes at interfaces: suitable materials, structures and properties. Macromol Rapid Commun. 2000;21:319–348.
[20] Zhu H, Ji J, Shan J. Construction of multilayer coating onto poly-(dl-lactide) to promote cytocompatibility. Biomaterials. 2004;25:109–117.
[21] Blasi P, Schoubben A, Traina G, et al. Lipid nanoparticles for brain targeting III. Long-term stability and in vivo toxicity. Int J Pharm. 2013;454:316–323.
[22] Vargas A, Zeisser-Labouèb M, Lange N, et al. The chick embryo and its chorioallantoic membrane (CAM) for the in vivo evaluation of drug delivery systems. Adv Drug Deliv Rev. 2007;59:1162–1176.
[23] Saw CLL, Heng PWS, Liew CV. Chick chorioallantoic membrane as an in situ biological membrane for pharmaceutical formulation development: a review. Drug Dev Ind Pharm. 2008;34:1168–1177.
[24] Altman R, Asch E, Bloch D, et al. Development of criteria for the classification and reporting of osteoarthritis. Classification of osteoarthritis of the knee. Diagnostic and Therapeutic Criteria Committee of the American Rheumatism Association. Arthritis Rheum. 1986;29:1039–1049.
[25] Oliveira MB, Mano JF. Polymer-based microparticles in tissue engineering and regenerative medicine. Biotechnol Progress. 2011;27:897–912.
[26] Vey E, Rodger C, Booth J, et al. Degradation kinetics of poly(lactic-co-glycolic) acid block copolymer cast films in phosphate buffer solution as revealed by infrared and Raman spectroscopies. Polym Degrad Stabil. 2011;96:1882–1889.
[27] Sun X, Wang J, Wang Y, et al. Collagen-based porous scaffolds containing PLGA microspheres for controlled kartogenin release in cartilage tissue engineering. Artif Cells Nanomed Biotechnol. 2017. DOI:10.1080/21691401.2017.1397000
[28] Li S. Hydrolytic degradation characteristics of aliphatic polyesters derived from lactic and glycolic acids. J Biomed Mater Res. 1999;48:342–353.

[29] Selmin F, Blasi P, DeLuca PP. Accelerated polymer biodegradation of risperidone poly(D, L-lactide-co-glycolide) microspheres. AAPS PharmSciTech. 2012;13:1465–1472.
[30] Guo C, Gemeinhart RA. Understanding the adsorption mechanism of chitosan onto poly(lactide-co-glycolide) particles. Eur J Pharm Biopharm. 2008;70:597–604.
[31] Wu L, Ding J. In vitro degradation of three-dimensional porous poly(d,l-lactide-coglycolide) scaffolds for tissue engineering. Biomaterials 2004;25:5821–5830.
[32] Pan Z, Ding J. Poly(lactide-co-glycolide) porous scaffolds for tissue engineering and regenerative medicine. Interface Focus. 2012;2: 366–377.
[33] Valdes TI, Kreutzer D, Moussy F. The chick chorioallantoic membrane as a novel in vivo model for the testing of biomaterials. J Biomed Mater Res. 2002;62:273–282.
[34] Schoubben A, Blasi P, Marenzoni ML, et al. Capreomycin supergenerics for pulmonary tuberculosis treatment: preparation, in vitro, and in vivo characterization. Eur J Pharm Biopharm. 2013;83:388–395.
[35] Romanoff AL. The Avian Embryo. Structural and functional development. New York (NY): The Macmillan Company; 1960.
[36] Kariminekoo S, Movassaghpour A, Rahimzadeh A, et al. Implications of mesenchymal stem cells in regenerative medicine. Artif Cells Nanomed Biotechnol. 2016;44:749–757.
[37] Fischer AH, Jacobson KA, Rose J, et al. Hematoxylin and eosin staining of tissue and cell sections. Cold Spring Harb Protoc. 2008;3:1–2.
[38] Weigel T, Schinkel G, Lendlein A. Design and preparation of polymeric scaffolds for tissue engineering. Expert Rev Med Devices. 2006;3:835–851.
[39] Loh QL, Choong C. Three-dimensional scaffolds for tissue engineering applications: role of porosity and pore size. Tissue Eng. Part B Rev.2013;19:485–502.
[40] Kaplan FS, Hayes WC, Keaveny TM, et al. Form and function of bone In: Simon SR editor. Orthopaedic basic science. Rosemont (IL): American Academy of Orthopaedic Surgeons; 1994: 127–84.
[41] Asa'ad F, Pagni G, Pilipchuk SP, et al. 3D-printed scaffolds and biomaterials: Review of alveolar bone augmentation and periodontal regeneration applications. Int J Dent. 2016;2016:1239842.
[42] Agrawal CM, Huang D, Schmitz JP, et al. Elevated temperature degradation of a 50:50 copolymer of PLA-PGA. Tissue Eng. 1997;3:345–352.
[43] Huang Z, Nelson ER, Smith RL, et al. The sequential expression profiles of growth factors from osteoprogenitors to osteoblasts in vitro. Tissue Eng. 2007;13:2311–2320.
[44] Birmingham E, Niebur GL, McHugh PE, et al. Osteogenic differentiation of mesenchymal stem cells is regulated by osteocyte and osteoblast cells in a simplified bone niche. Eur Cell Mater.2012;23:13–27.
[45] Cai X, Su X, Li G, et al. Osteogenesis of adipose-derived stem cells. In: Lin Y editor. Osteogenesis. Croatia: In Tech d.o.o.; 2012 pp 135–52.